Efficient water-based purification of metal-organic polyhedra by centrifugal ultrafiltration

Benjamin Le Ouay,*[a] Tomo Ohara,[a] Ryosuke Minami,[a] Rin Kunitomo,[a] Ryo Ohtani, [a] Masaaki Ohba*[a]

[a] *Department of Chemistry, Graduate School of Science, Kyushu University, 744 Motooka, Nishi-ku, Fukuoka 819-0395, Japan.*

Materials and methods

Ultrafiltration membranes

Sample purification was performed using Amicon® Ultra-15 centrifugal ultrafiltration units, with nominal molecular weight cut-off (MWCO) of 10 kDa (Merck-Millipore). In this case, membrane are constituted of regenerated cellulose. Amicon® Ultra-4 were also used when filtration of smaller volumes was more appropriate, notably during permeation tests. Permeation using Amicon® Ultra-4 with a nominal MWCO of 100 kDa wa also evaluated.

In addition, MOP permeation using ultrafiltration units with a MWCO of 100 kDa (AS ONE, material: Polyethersulfone) and with a MWCO of 1 MDa (Vivaspin® 20, Sartorius, material: Polyethersulfone) was also evaluated.

Rhodium (II) acetate dimer and Sodium 3,5-dicarboxybenzenesulfonate (H_2**ip–SO_3**) were obtained from TCI chemicals. Sodium 6-(3,5-dicarboxyphenoxy)-hexane-1-sulfonate (H_2**ip–C_6SO_3**) and 6-(3,5-dicarboxyphenoxy)-N,N,N-trimethylhexan-1-aminium chloride (H_2**ip–C_6NMe_3**) were prepared as previously reported.[1]

MOP syntheses and purification

Synthesis of Rh–SO_3

Rhodium (II) acetate dimer ($Rh_2(OAc)_4$, 0.1 mmol, 44 mg), H_2**ip-SO_3** (0.4 mmol, 107 mg), sodium carbonate (0.4 mmol, 42 mg), 3 ml dimethylacetamide (DMA) and 0.3 ml water were introduced in a glass vial, dispersed by ultrasonication for 10 minutes, then maintained at 65 °C for 72h. After that, **Rh–SO_3** was purified using the general procedure (see below). Yield: 56% (based on rhodium). Elemental analysis, calculated for Rh_{24}(**ip-SO_3**)$_{24}$· 10MeOH· 10H_2O ($Rh_{24}C_{202}H_{132}S_{24}O_{188}Na_{24}$): H: 1.42%; C: 25.93%; N: 0.00%. Observed: H: 1.36%; C: 25.86%; N: 0.03%.

Synthesis of Rh–C_6SO_3

Rhodium (II) acetate dimer ($Rh_2(OAc)_4$, 0.1 mmol, 44 mg), H_2**ip-C_6SO_3** (0.4 mmol, 147 mg), sodium carbonate (0.4 mmol, 42 mg), 3 ml dimethylacetamide (DMA) and 0.3 ml water were introduced in a glass vial, dispersed by ultrasonication for 10 minutes, then maintained at 65 °C

for 72h. After that, **Rh–C_6SO_3** was purified using the general procedure (see below). Yield: 67% (based on rhodium). Elemental analysis, calculated for Rh_{24}(**ip-C_6SO_3**)$_{24}$ ($Rh_{24}C_{336}H_{360}S_{24}O_{192}Na_{24}$): H: 3.22%; C: 35.84%; N: 0.00%. Observed: H: 3.50%; C: 36.06%; N: 0.00%.

Synthesis of Rh–C_6NMe_3

Rhodium (II) acetate dimer ($Rh_2(OAc)_4$, 0.1 mmol, 44 mg), H_2**ip-C_6NMe_3** (0.4 mmol, 144 mg), sodium carbonate (0.4 mmol, 42 mg), 3 ml dimethylacetamide (DMA) and 0.3 ml water were introduced in a glass vial, dispersed by ultrasonication for 10 minutes, then maintained at 65 °C for 72h. After that, **Rh–C_6NMe_3** was purified using the general procedure (see below). Yield: 69% (based on rhodium). Elemental analysis, calculated for Rh_{24}(**ip-C_6NMe_3**)$_{24}$·$20H_2O$ ($Rh_{24}C_{408}H_{616}N_{24}O_{140}Cl_{24}$): H: 5.44%; C: 42.92%; N: 2.94%. Observed: H: 5.54%; C: 43.01%; N: 2.73%.

Procedure for the purification and isolation of **Rh–SO_3**; **Rh–C_6SO_3** and **Rh–C_6NMe_3**

After the reaction was complete, diethyl ether (ca. 100 ml) was added to the reaction mixture, causing the precipitation of all relevant species. In particular, the diethylether/DMA solution was colorless, indicating that all Rh-containing species were precipitated. The precipitate was then filtered, washed with diethyl ether and collected by filtration, before being redissolved in water (ca. 80 ml). In order to regulate pH and ionic species, 20 ml of a concentrated sodium hydrogen carbonate solution were added to **Rh–SO_3** and **Rh–C_6SO_3**. Meanwhile, the pH of **Rh–C_6NMe_3** was adjusted to 2.0 using HCl (4 mol/l). In this manuscript, these are refered as the reaction mixtures.

Crude solutions were filtered using a hydrophilic PTFE membrane (pore size: 0.1 mm) before being submitted to several centrifugal ultrafiltration cycles. Since the volume of the filter body was only 15 ml, the crude solution was introduced in several times. After all the crude solution was introduced, samples were washed multiple times using deionized water (at least 5 cycles), until the filtrates presented acceptably low absorbances (See Figure S5). Concentrated MOP solutions were then evaporated under reduced pressure. To dry more efficiently the very hydrophilic MOPs, toluene was added to the flasks then evaporated until dry looking powders were obtained (toluene-water azeotropic distillation). MOPs powders were dissolved in a minimal amount of anhydrous methanol (ca. 5 ml), then precipitated with 150 ml of diethyl ether and collected by filtration, before being dried under high vacuum (5 Pa for 24h). Note that this drying process introduces a few strongly coordinated methanol and diethyl ether molecules on the MOP (see Figure S7). These solvent molecules can however easily be displaced by dissolution in water.

Note also that the centrifugal filters were able to accommodate significantly larger batches than described (up to 0.5 mmol of rhodium acetate dimer per batch) without preventing transport. In some cases, concentrated MOP solutions can have a jelly-like texture that clogs the filter. To remedy this, MOPs can be redispersed in a large volume of water before being re-filtered. A 20 v% ethanol solution can also be used to help disperse MOPs without damaging performances of the filter.

Procedure for cation exchange on **Rh–SO_3**

Exchange was performed with the following species: potassium nitrate, triflic acid, tetraethylammonium chloride and magnesium perchlorate. A stock solution of the correpsonding salt (1 mol/L in water) was prepared. 10 mg of **Rh–SO_3** (counter-ion: Na^+) were dissolved in 2 ml water, then introduced in the ultrafiltration unit, as well as 13 ml of salt solution, before being centrifugated. Salt solution was then replaced and filtered three more time to further ion exchange. After this, MOPs were washed five time with deionized water. The MOP solution was then transferred in a vial and dried at 80 °C. In the case of H^+-exchanged **Rh–SO_3** was treated in a quartz cuvette, in order to prevent Na^+ leaching from glass.

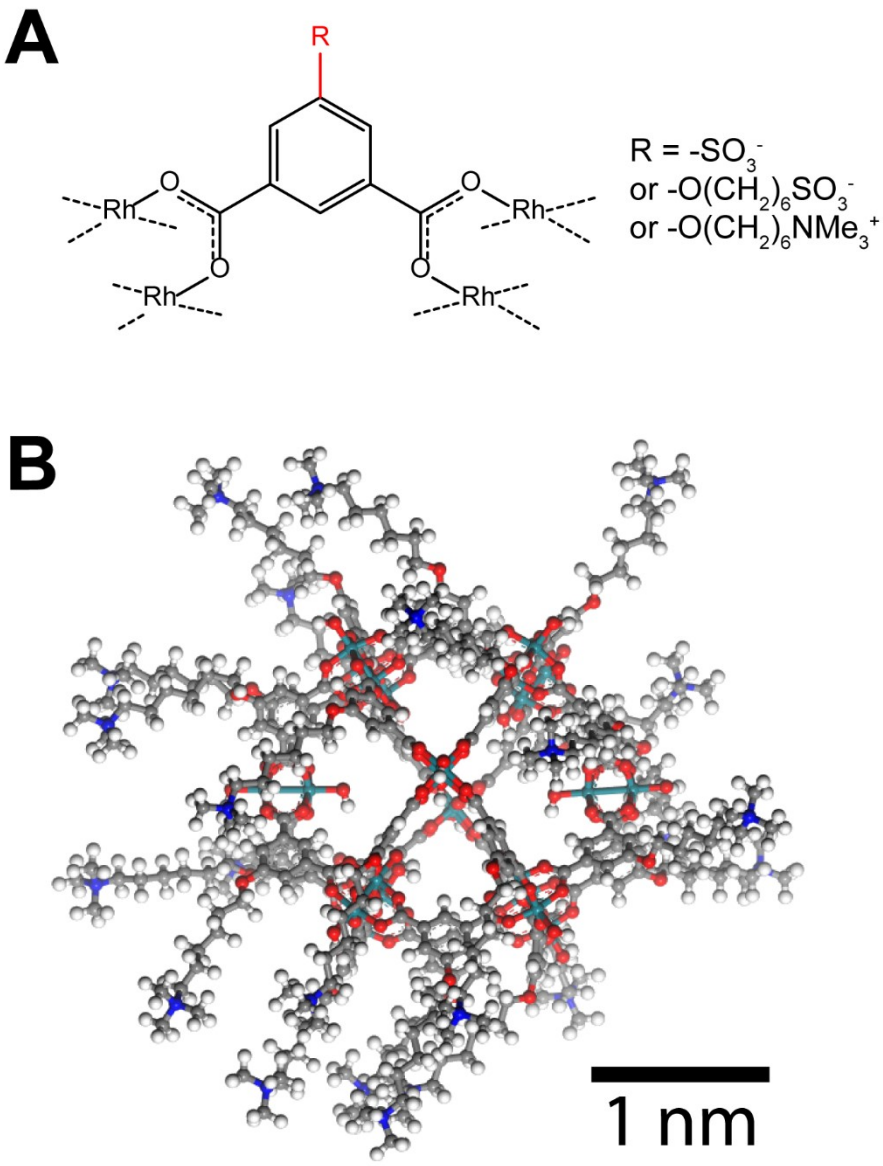

Figure S1. A: Ligand structure and coordination of the $Rh_{24}(ip)_{24}$-derived MOPs used in this work. **B**: Structural model of a $Rh_{24}(ip)_{24}$-derived MOP. Here, **Rh–C_6NMe_3** is shown.

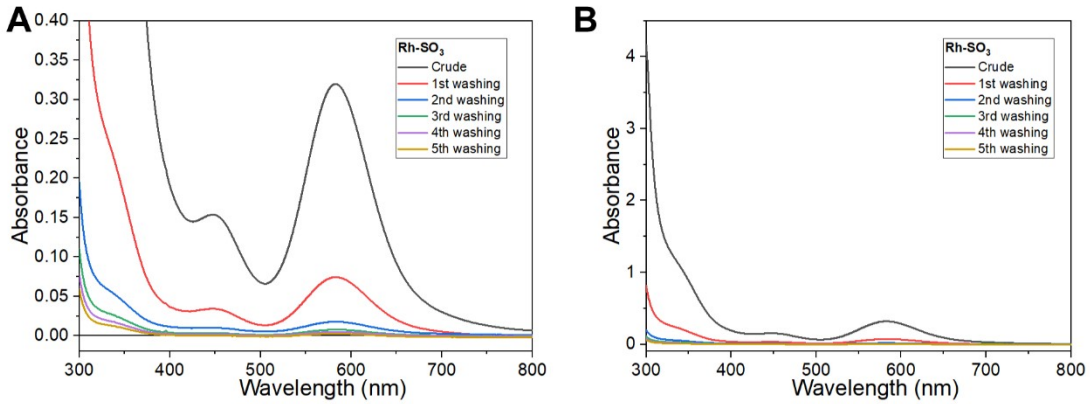

Figure S2. UV-Visible absorbance spectra of crude **Rh–SO_3** solution and filtrates obtained after repeated washings with water. **A** and **B** show different Y-axis scales to emphasize the Rh-related absoption around 600 nm and 450 nm, or the ligand-related absorption below 350 nm.

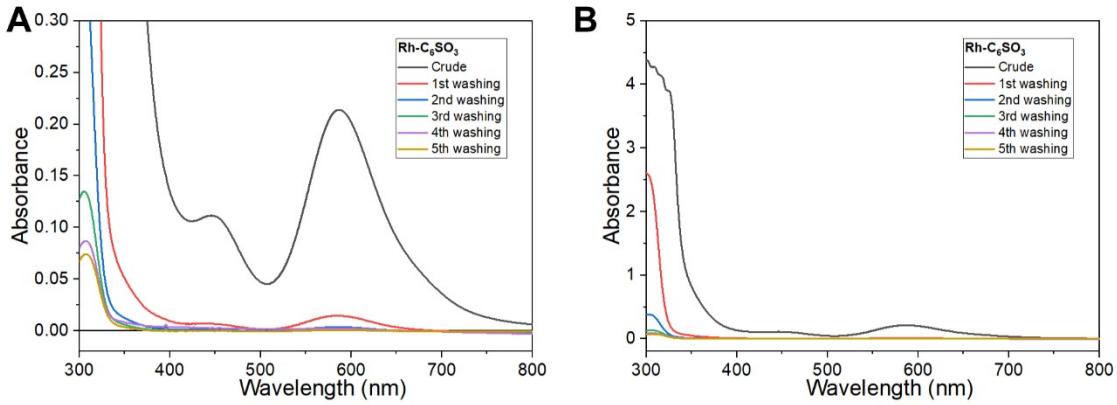

Figure S3. UV-Visible absorbance spectra of crude **Rh–C_6SO_3** solution and filtrates obtained after repeated washings with water. **A** and **B** show different Y-axis scales to emphasize the Rh-related absoption around 600 nm and 450 nm, or the ligand-related absorption below 350 nm.

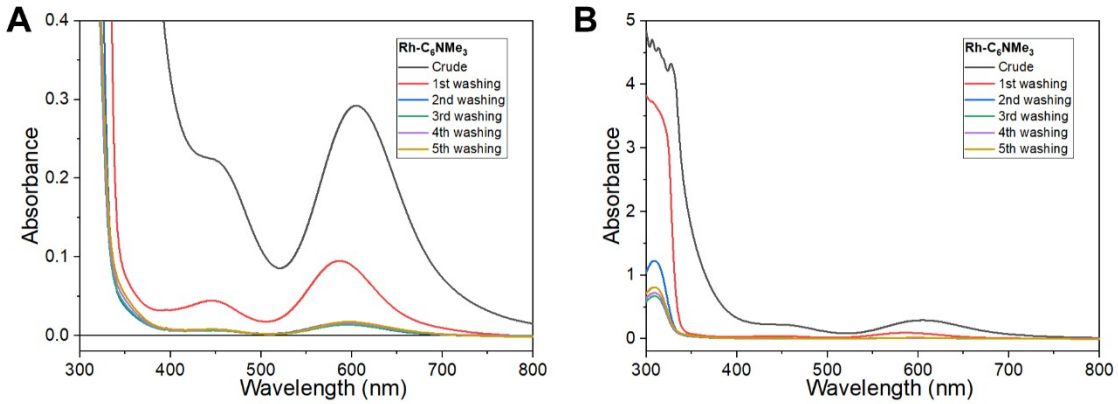

Figure S4. UV-Visible absorbance spectra of crude **Rh–C_6NMe$_3$**solution and filtrates obtained after repeated washings with water. **A** and **B** show different Y-axis scales to emphasize the Rh-related absoption around 600 nm and 450 nm, or the ligand-related absorption below 350 nm.

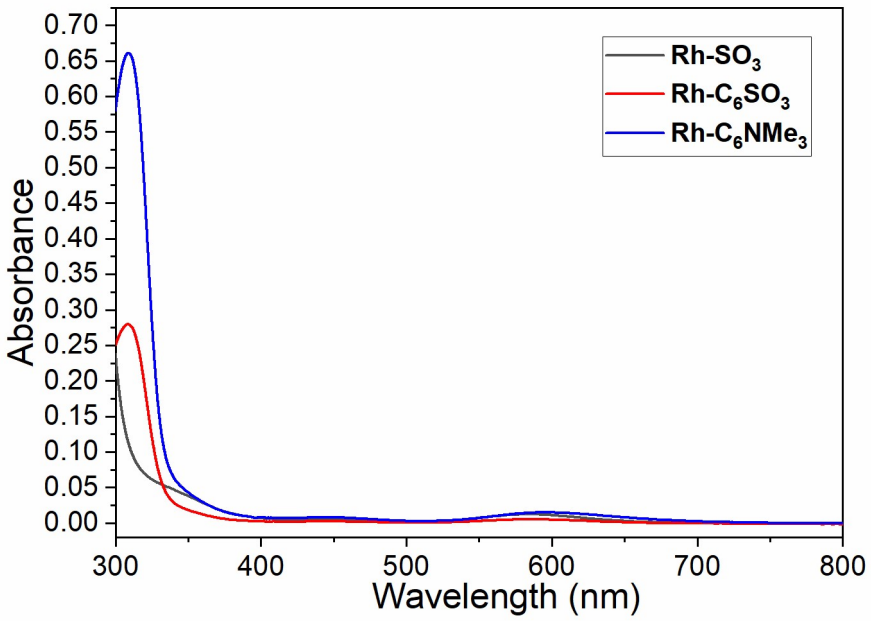

Figure S5. UV-visible spectra of the last filtrates obtained before evaporation and storage of **Rh–SO_3**; **Rh–C_6SO_3** and **Rh–C_6NMe_3**. The presence of residual absorbance bands in the filtrates despite thorough washings may originate either from an imperfect retention by the membrane, or from a slight dissociation of Rh-MOPs in pure water. Note that since full synthesis batch were introduced in the filter, the concentration of the MOP solution in the filter is significantly than for Figures S2 to S4.

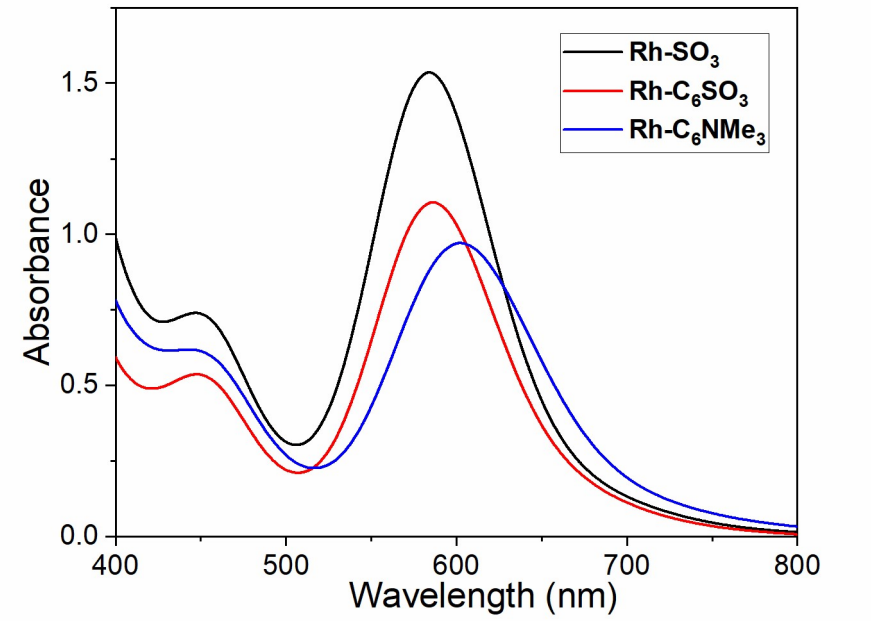

Figure S6. UV-visible absorbance spectra of solutions of **Rh–SO_3**, **Rh–C_6SO_3** and **Rh–C_6NMe_3** prepared from redissolved powders. Concentration: 5 mg/ml.

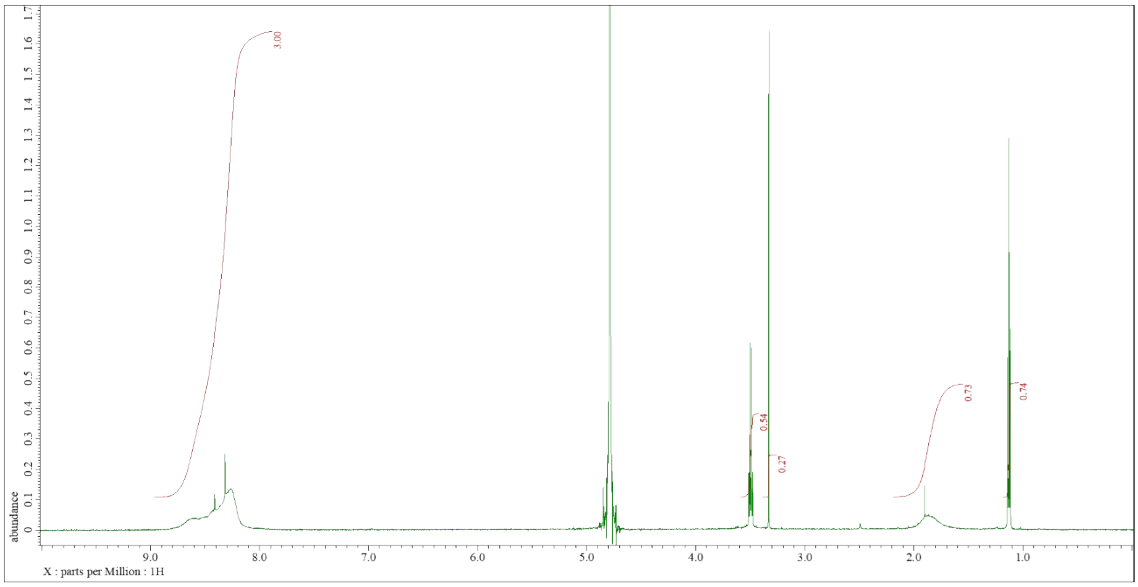

Figure S7. ^{1}H-NMR spectrum of as synthesized **Rh–SO$_3$**. Despite thorough degassing, sharp peaks corresponding to methanol (3.34 ppm) and diethyl ether (1.17 ppm and 3.56 ppm) were observed, indicating strongly coordinated species on the Rh paddlewheels. Despite their high maximum intensities, these sharp peaks have a comparably low integral compared to the broad peaks originating from the MOP ligands. This peak broadening for ligands on MOPs was attributed to a slow rotation of the cage at the scale of the NMR analysis.[2,3] The methanol and diethyl ether peaks can be suppressed by dissolving the MOP in ca. 100 µl of D_2O (causing a coordination displacement), then evaporating this solvent and measuring the spectrum in fresh D_2O (See Figure S8).

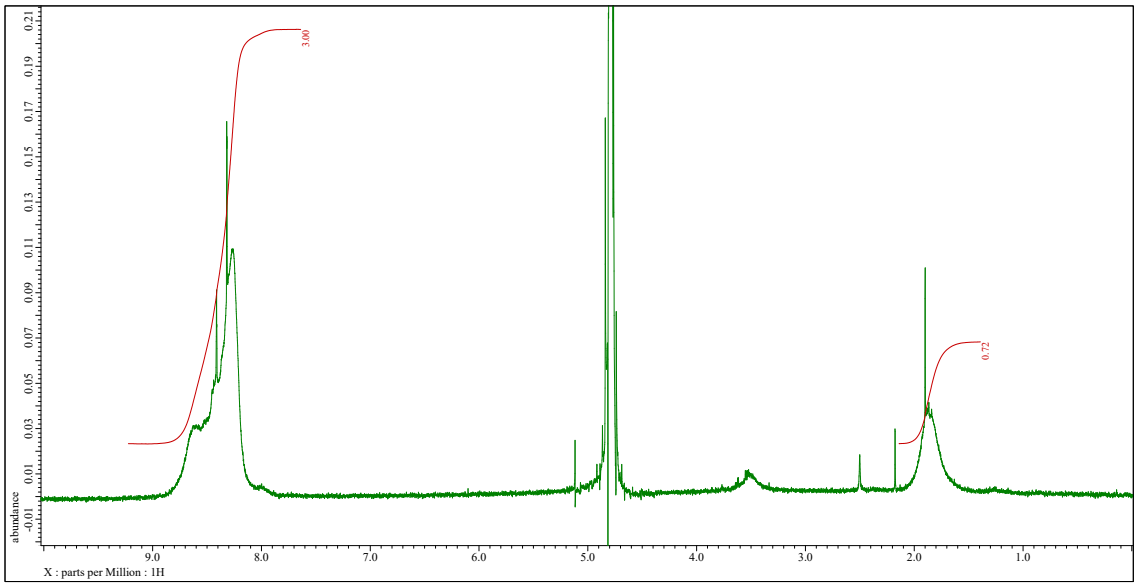

Figure S8. ^{1}H-NMR spectrum of **Rh–SO$_3$** with peaks of volatile species suppressed. The broad peak of coordinated **ip–SO$_3$** (8-9 ppm) was observed. This peak broadening for ligands on MOPs was attributed to a slow rotation of the cage at the scale of the NMR analysis.[2,3] Another broad peak around 2 ppm was observed, and may correspond to coordination defects and a substitution of some **ip–SO$_3$** by acetates. Minor peaks corresponding to free ligands were also observed (See Figure S9).

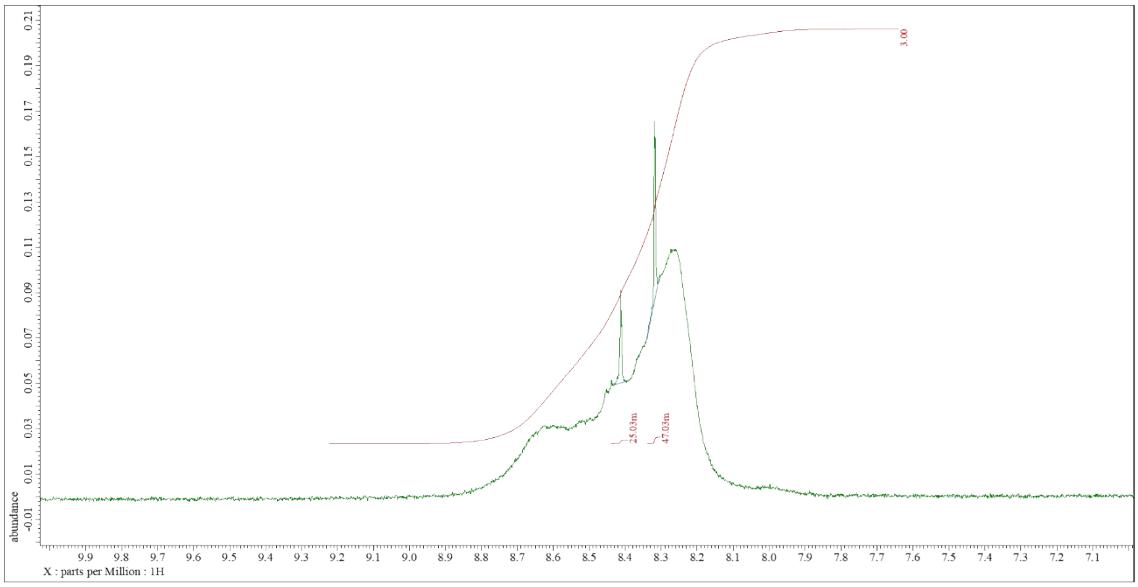

Figure S9. ^{1}H-NMR spectrum of **Rh–SO$_3$**: zoom on the aromatic region. 2 minors peaks corresponding to free ligands were also observed. However, the low value of their combined integrals (0.072) compared to that of the broad peak (set as 3.00) indicates that MOPs has a purity of > 97%.

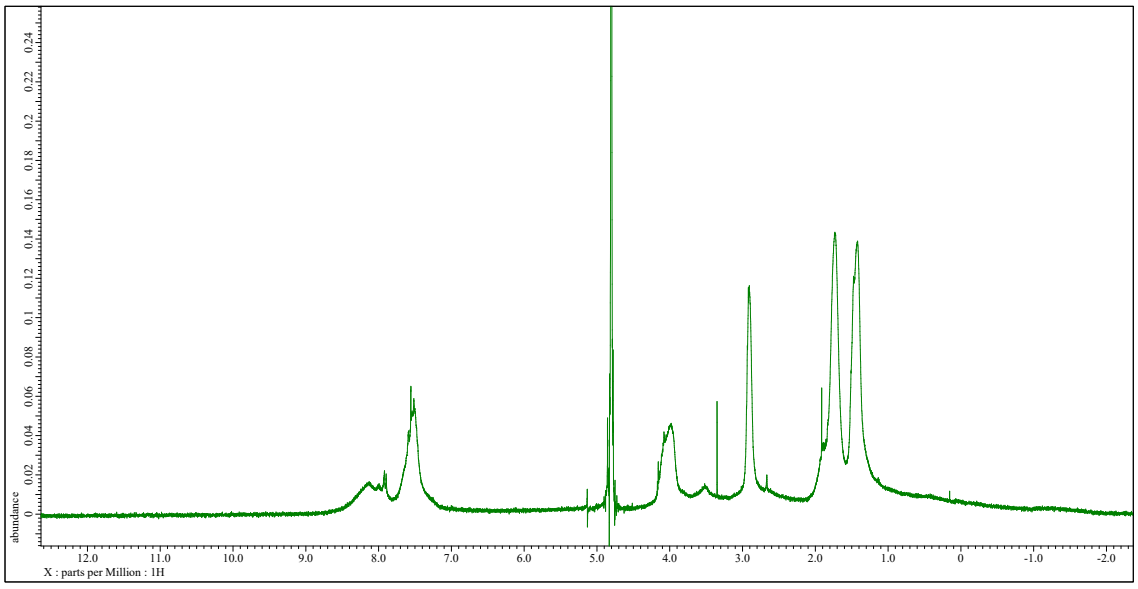

Figure S10. ^{1}H-NMR spectrum of **Rh–C$_6$SO$_3$** with peaks of volatile species suppressed.

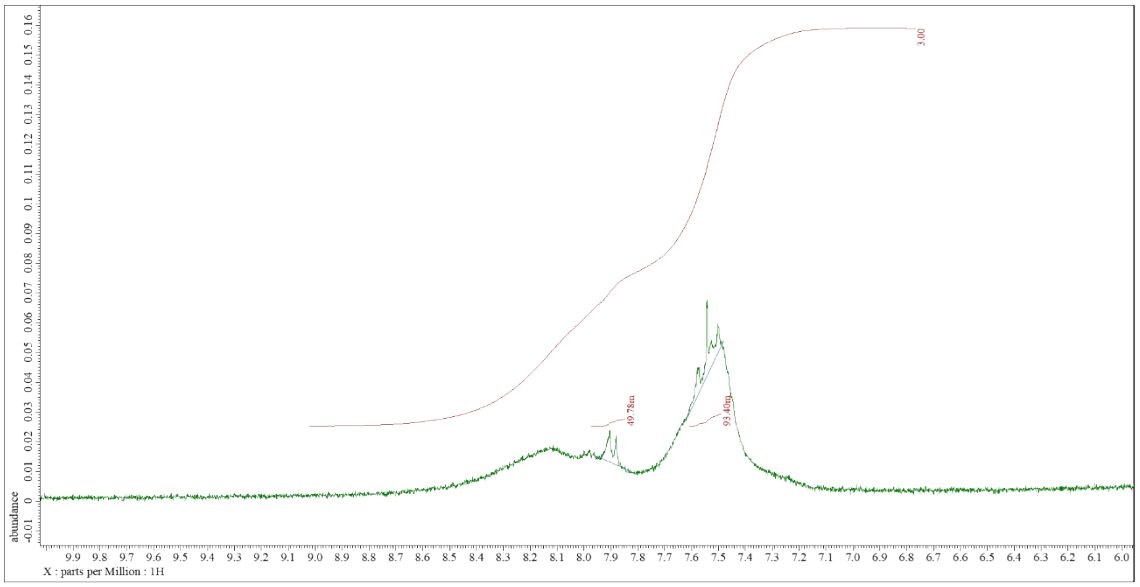

Figure S11. ^{1}H-NMR spectrum of **Rh–C_6SO_3**: zoom on the aromatic region. Sharp peaks were observed, indicating the presence of free ligands. However, the low value of their combined integrals (0.143) compared to that of the broad peak (set as 3.00) indicates that MOPs has a purity of > 95%.

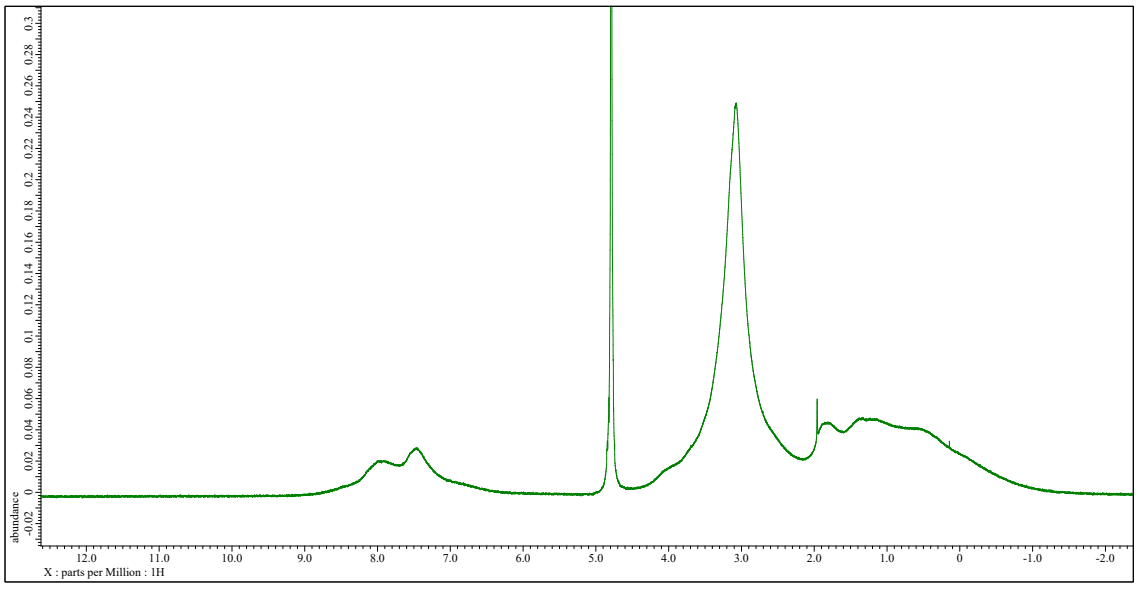

Figure S12. ^{1}H-NMR spectrum of **Rh–C_6NMe_3** with peaks of volatile species suppressed. In this sample, peaks of free ligands were not detected.

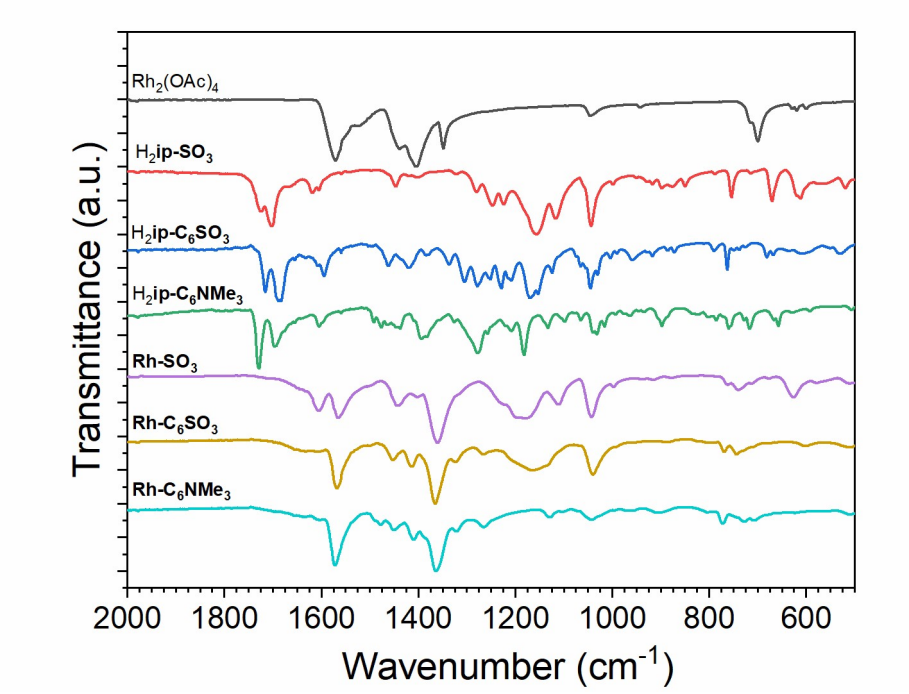

Figure S13. Fourier transform infrared (FTIR) spectra of **Rh–SO_3**, **Rh–C_6SO_3**, **Rh–C_6NMe_3** and their precursors. Formation of the MOPs is indicated by the disappearance of peaks corresponding to carboxylic acid groups (around 1700 cm^{-1}) and the appearance of peaks related to the Rh-carboxylate paddlewheels, around 1560 cm^{-1} and 1370 cm^{-1}.

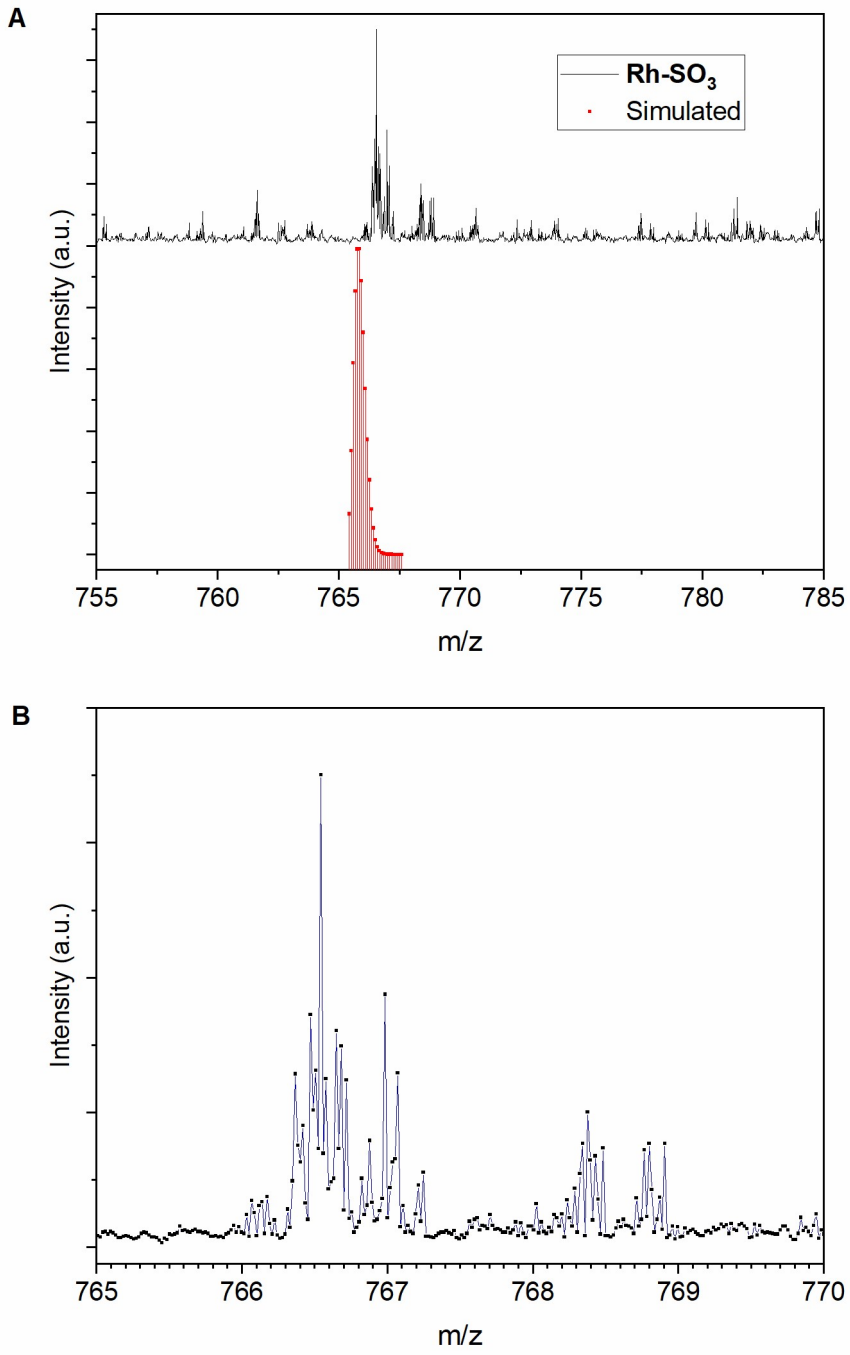

Figure S14. A: ESI-TOF spectrum of **Rh-SO_3** in MeOH (Negative mode), and a simulation pattern for $[Na_{12}$**Rh-SO_3**$\cdot 19\ MeOH]^{12-}$. **B**: Zoomed view of the peak region. Since the cages are polycharged species with a trend to form various adducts with strongly coordinated solvent molecules, the signal of the completely ionized and desolvated cage (charge 24-) could not be observed. However, the ESI-TOF spectra presented several narrow domains (width around 1 m/z unit) where many peaks were observed, which is compatible with the signal of a polycharged cage.

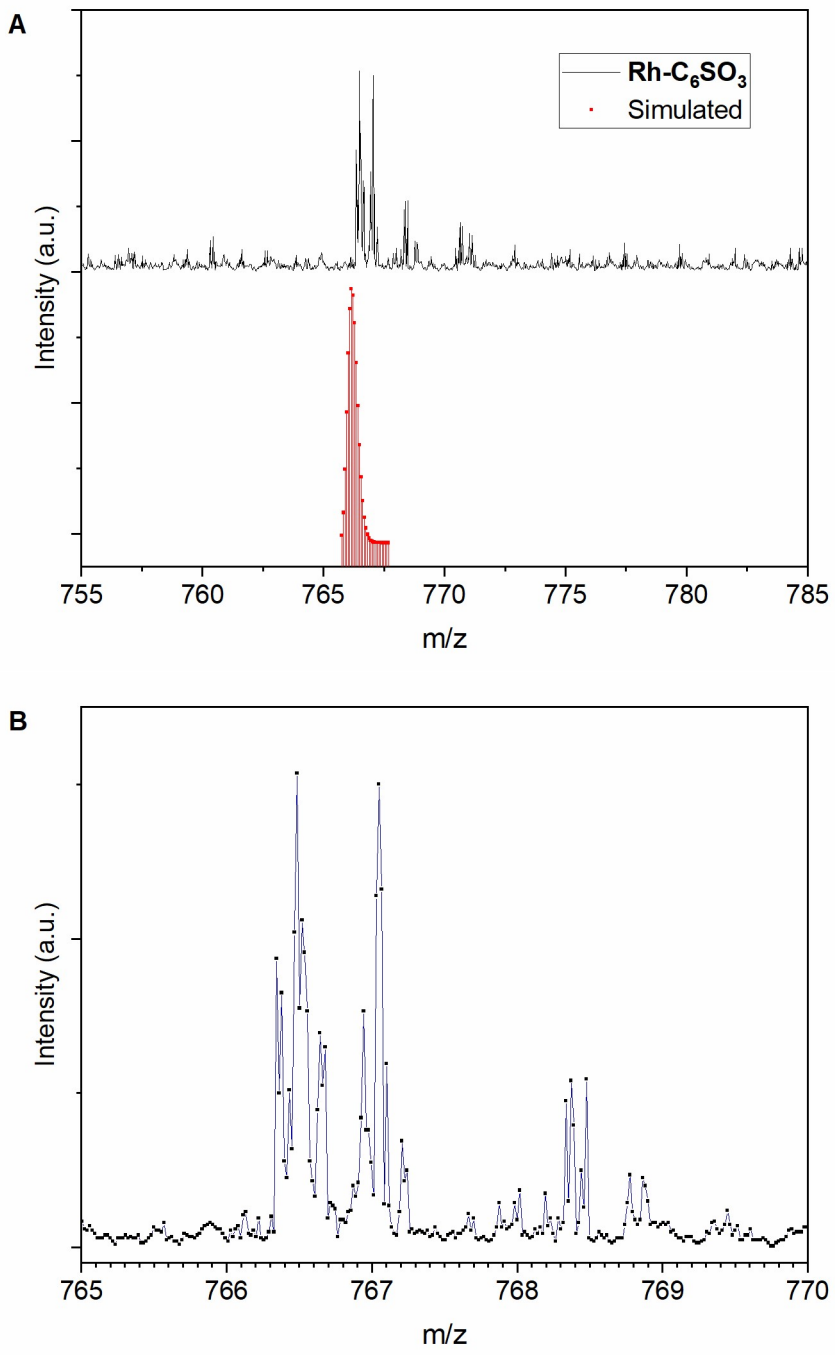

Figure S15. A: ESI-TOF spectrum of **Rh-C_6SO_3** in MeOH (Negative mode), and a simulation pattern for [Na_9**Rh-C_6SO_3**·18 MeOH]$^{15-}$. **B**: Zoomed view of the peak region. Since the cages are polycharged species with a trend to form various adducts with strongly coordinated solvent molecules, the signal of the completely ionized and desolvated cage (charge 24-) could not be observed. However, the ESI-TOF spectra presented several narrow domains (width around 1 m/z unit) where many peaks were observed, which is compatible with the signal of a polycharged cage.

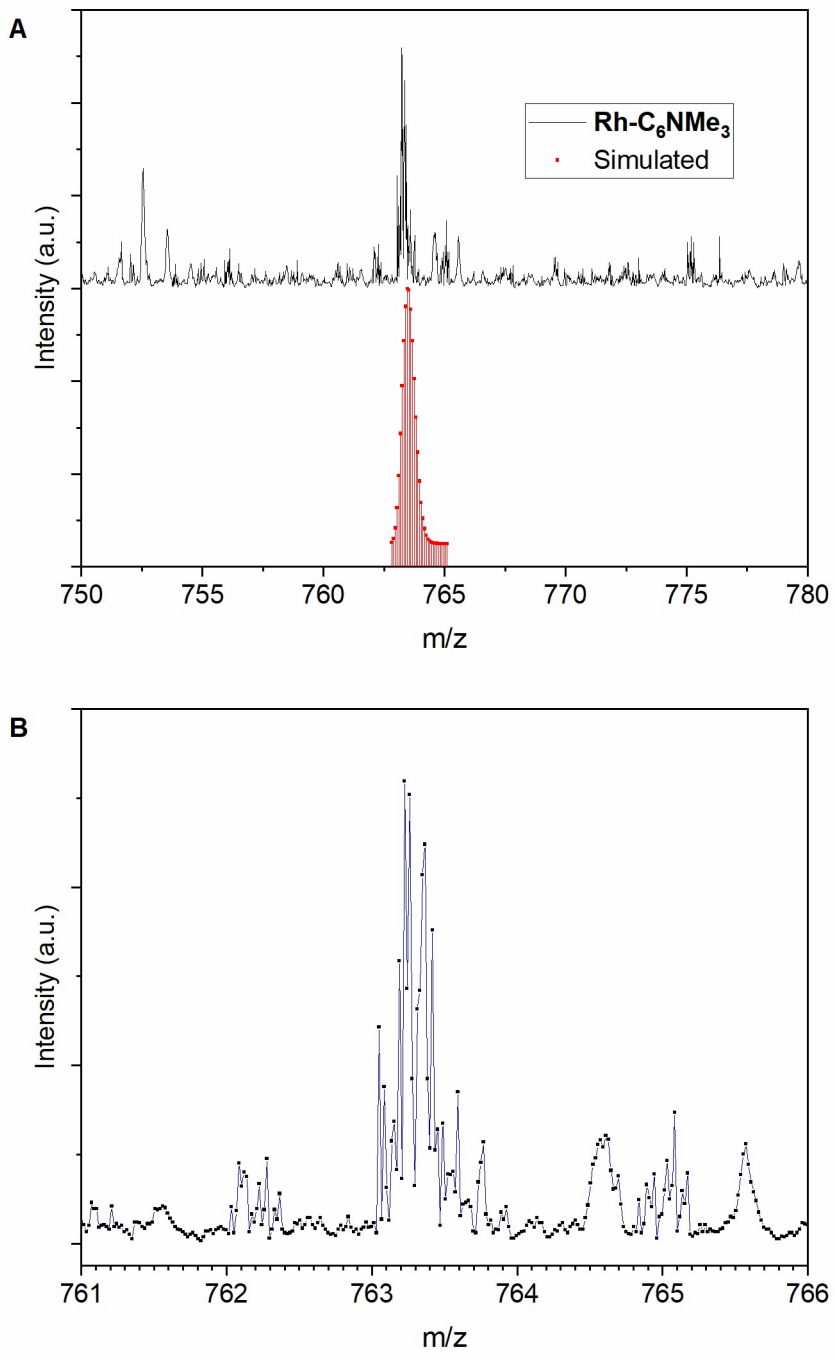

Figure S16. A: ESI-TOF spectrum of **Rh-NMe$_3$** in MeOH (Positive mode), and a simulation pattern for [**Rh-C$_6$SO$_3$**Cl$_{10}$·4 MeOH]$^{14+}$. **B**: Zoomed view of the peak region. Since the cages are polycharged species with a trend to form various adducts with strongly coordinated solvent molecules, the signal of the completely ionized and desolvated cage (charge 24+) could not be observed. However, the ESI-TOF spectra presented several narrow domains (width around 1 m/z unit) where many peaks were observed, which is compatible with the signal of a polycharged cage.

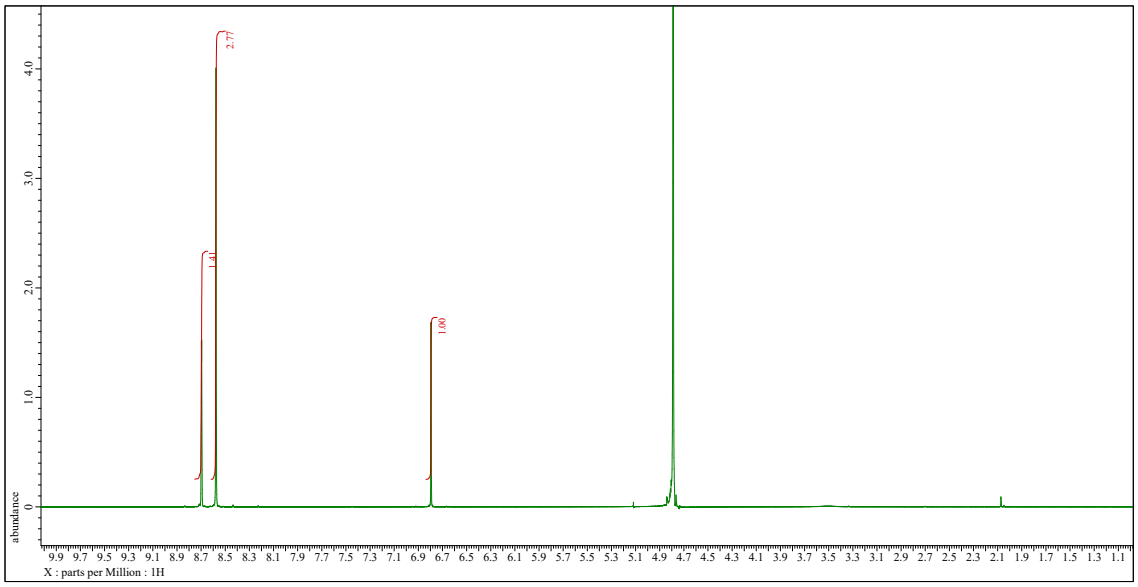

Figure S17. Permeation test for the ligand H_2**ip–SO$_3$**. ^{1}H-NMR spectrum of a solution before ultrafiltration. Fumaric acid (1 mg/ml, peak at 6.77 ppm) is used as an internal concentration reference. When setting the intensity of the fumaric acid peak to 1, the intensity of the peak for the proton between two carboxylic acids (8.69 ppm) was 1.41.

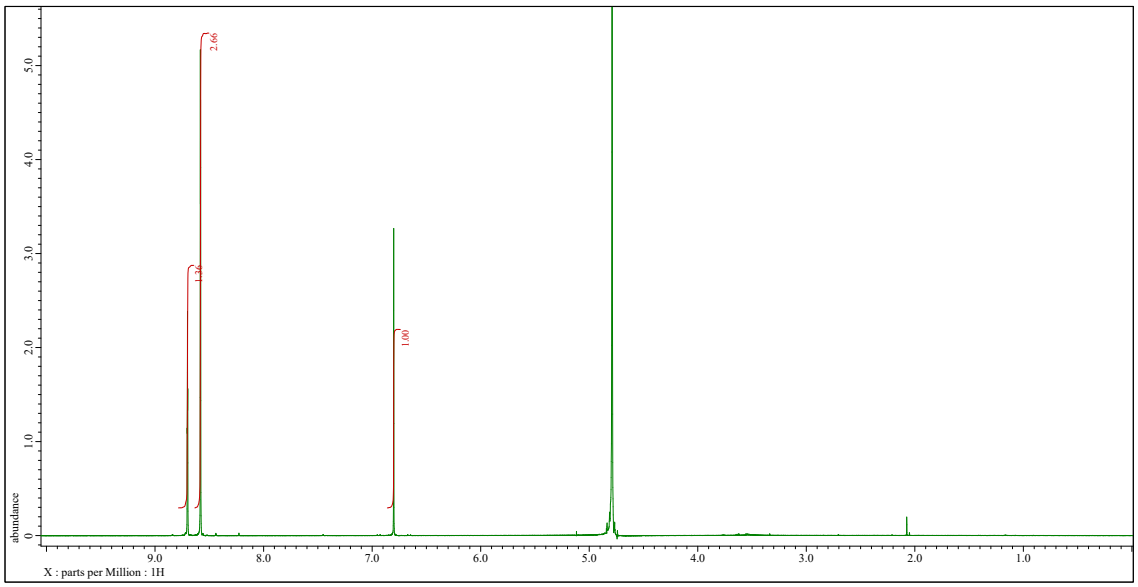

Figure S18. Permeation test for the ligand H_2**ip–SO$_3$**. ^{1}H-NMR spectrum of a solution after ultrafiltration. Fumaric acid (1 mg/ml, peak at 6.77 ppm) is used as an internal concentration reference. When setting the intensity of the fumaric acid peak to 1, the intensity of the peak for the proton between two carboxylic acids (8.69 ppm) was 1.36. This corresponds to a permeation coefficient of 96%.

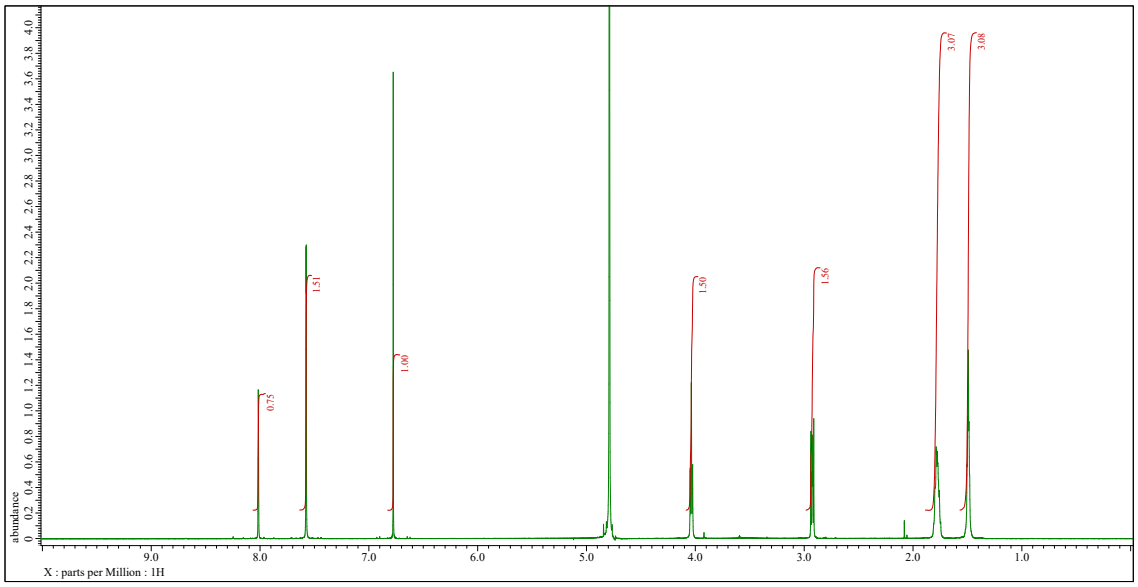

Figure S19. Permeation test for the ligand H_2**ip–C_6SO_3**. ^{1}H-NMR spectrum of a solution before ultrafiltration. Fumaric acid (1 mg/ml, peak at 6.77 ppm) is used as an internal concentration reference. When setting the intensity of the fumaric acid peak to 1, the intensity of the peak for the proton between two carboxylic acids (8.01 ppm) was 0.75.

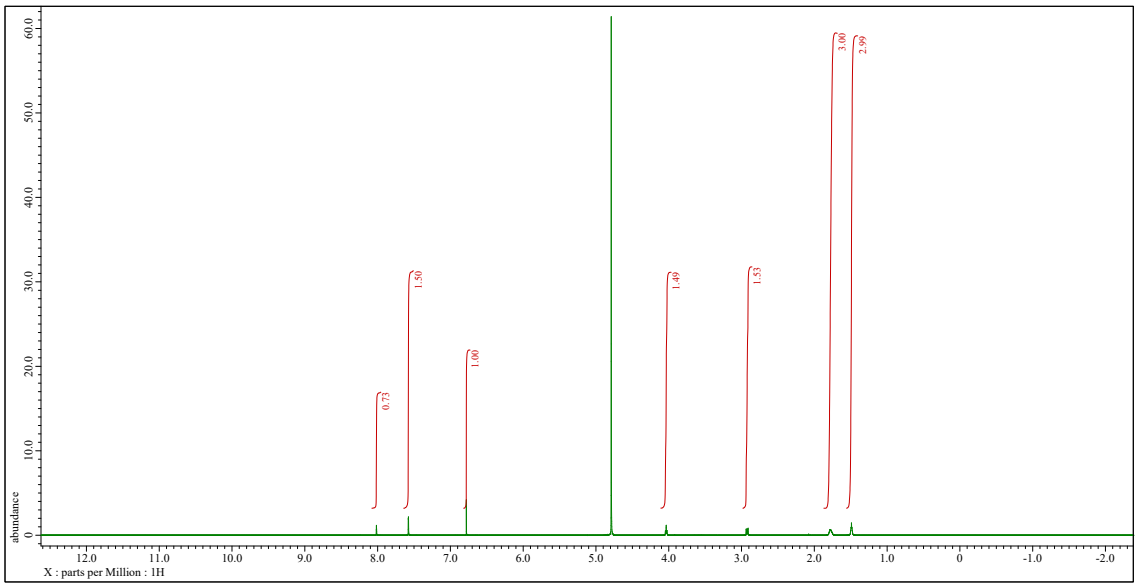

Figure S20. Permeation test for the ligand H_2**ip–C_6SO_3**. ^{1}H-NMR spectrum of a solution after ultrafiltration. Fumaric acid (1 mg/ml, peak at 6.77 ppm) is used as an internal concentration reference. When setting the intensity of the fumaric acid peak to 1, the intensity of the peak for the proton between two carboxylic acids (8.01 ppm) was 0.73. This corresponds to a permeation coefficient of 97%.

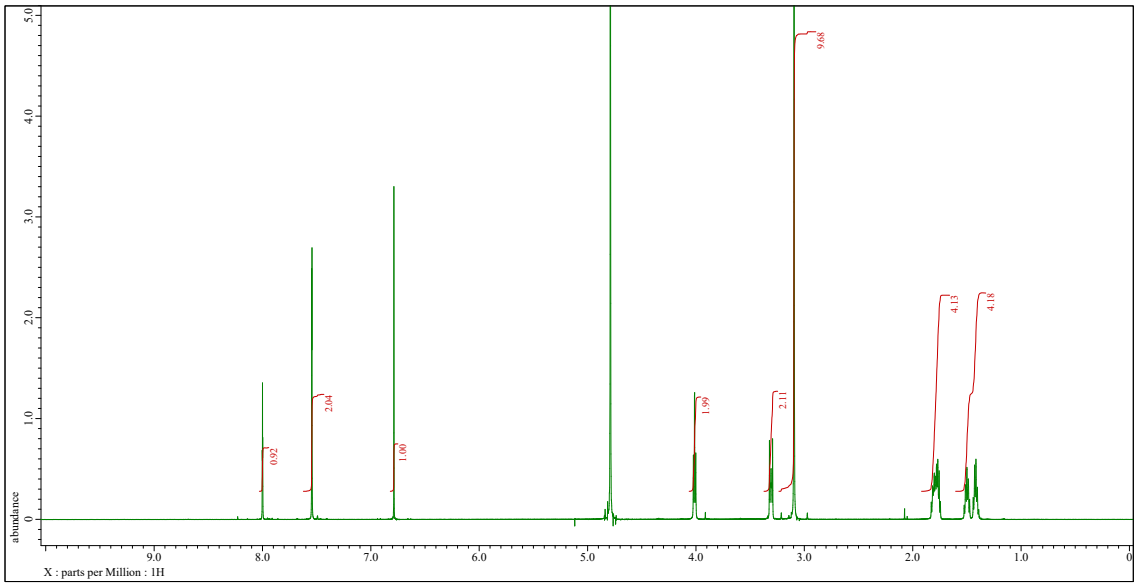

Figure S21. Permeation test for the ligand H_2**ip–C_6NMe$_3$**. ^{1}H-NMR spectrum of a solution before ultrafiltration. Fumaric acid (1 mg/ml, peak at 6.77 ppm) is used as an internal concentration reference. When setting the intensity of the fumaric acid peak to 1, the intensity of the peak for the proton between two carboxylic acids (8.00 ppm) was 0.92.

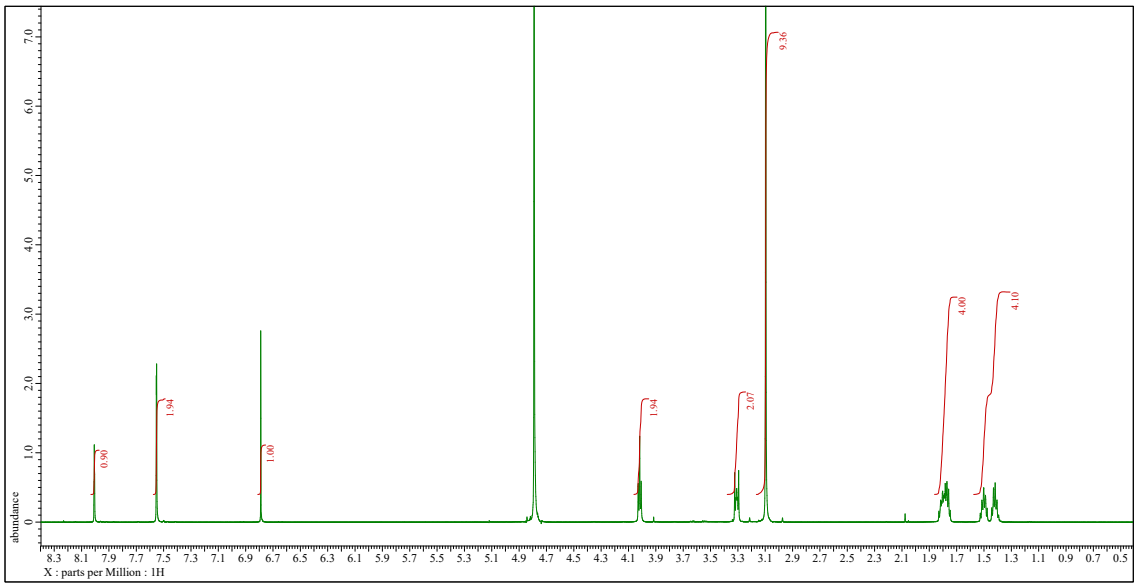

Figure S22. Permeation test for the ligand H_2**ip–C_6NMe$_3$**. ^{1}H-NMR spectrum of a solution after ultrafiltration. Fumaric acid (1 mg/ml, peak at 6.77 ppm) is used as an internal concentration reference. When setting the intensity of the fumaric acid peak to 1, the intensity of the peak for the proton between two carboxylic acids (8.00 ppm) was 0.90. This corresponds to a permeation coefficient of 98%.

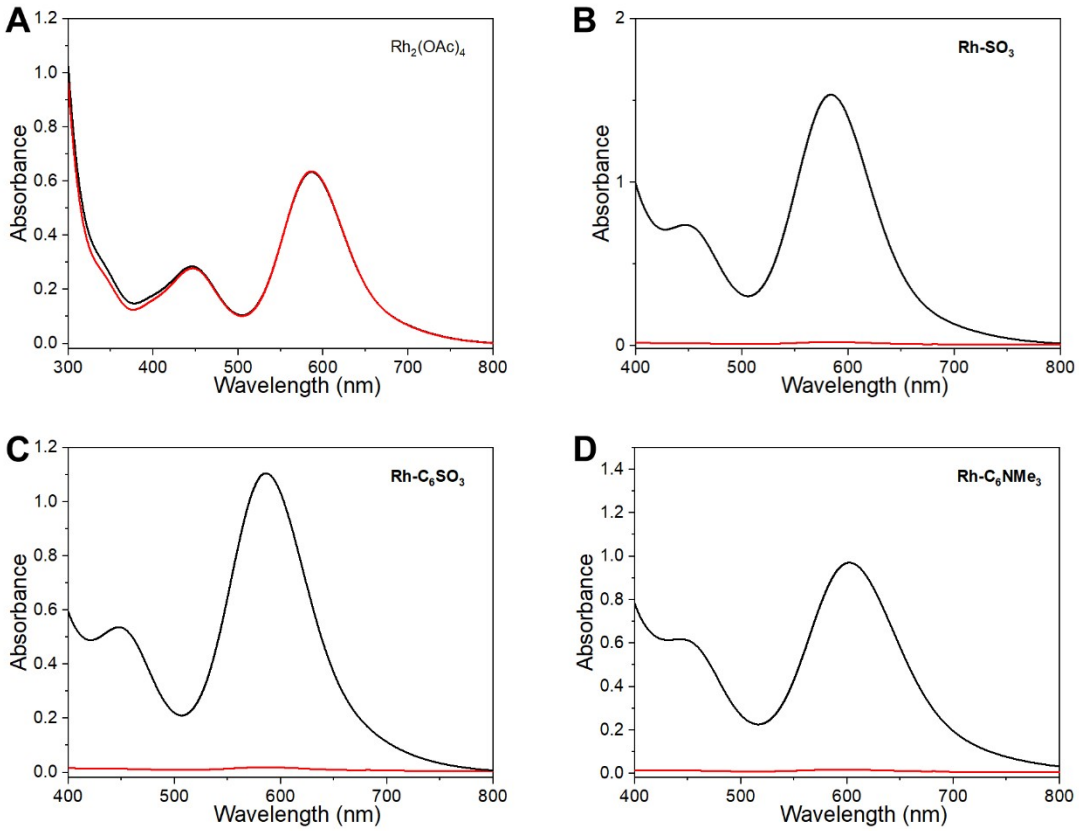

Figure S23. Determination of the permeation coefficient for ultrafiltration membranes with a molecular weight cut-off of 10 kDa. Membrane material in this case was regenerated cellulose. For Rh-containing species, UV-visible absorbance spectroscopy was used, using the decrease of Rh-related band intensities. Black: Initial solution. Red: Filtrate. **A**: Rhodium (II) acetate dimer, Permeation: 100 %. **B**: **Rh–SO_3**, Permeation: 1.5 %. **C**: **Rh–C_6SO_3**, Permeation: 1.7 %. **D**: **Rh–C_6NMe_3**, Permeation: 1.8 %.

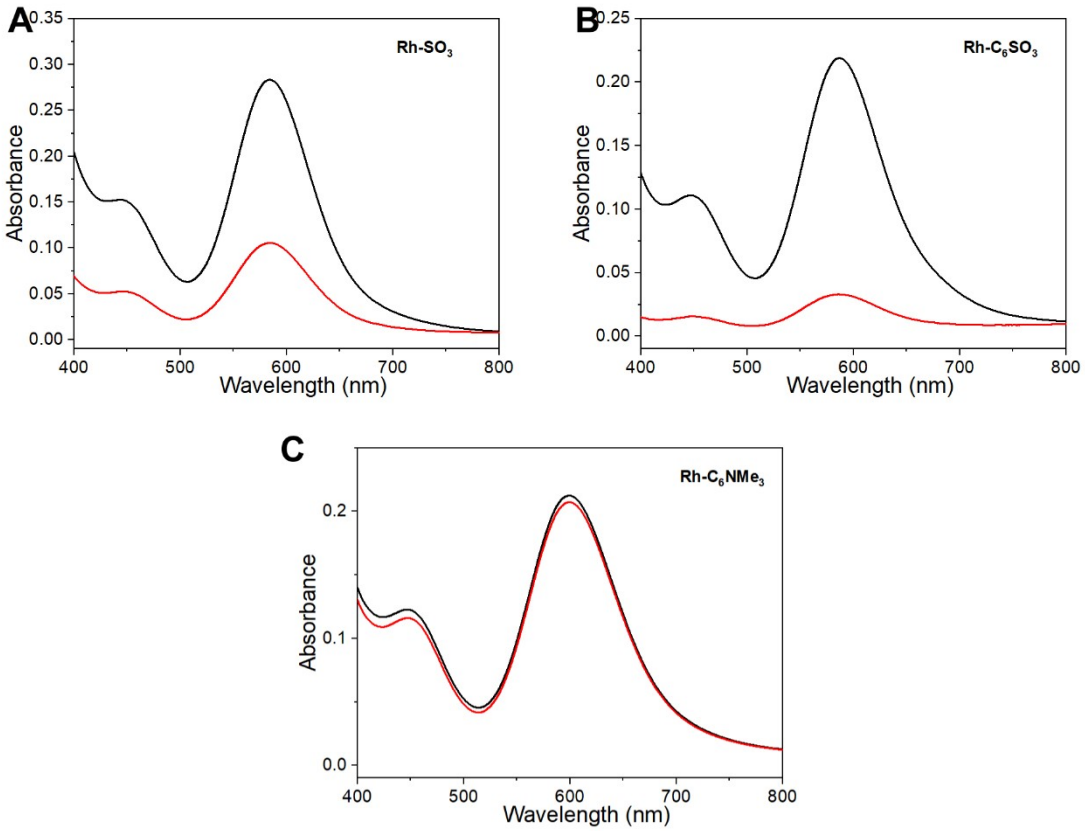

Figure S24. Determination of the permeation coefficient for ultrafiltration membranes with a molecular weight cut-off of 100 kDa. Membrane material in this case was regenerated cellulose. Black: Initial solution. Red: Filtrate. **A**: **Rh–SO_3**, Permeation: 37 %. **B**: **Rh–C_6SO_3**, Permeation: 15 %. **C**: **Rh–C_6NMe_3**, Permeation: 97 %.

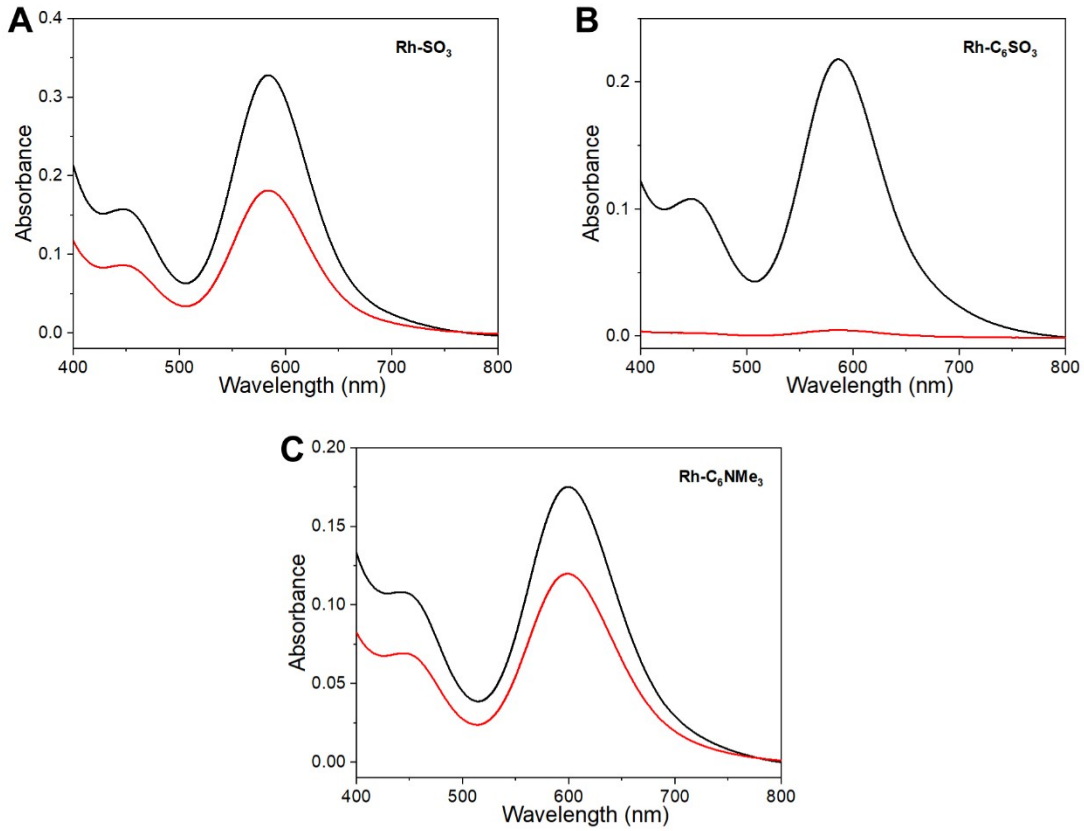

Figure S25. Determination of the permeation coefficient for ultrafiltration membranes with a molecular weight cut-off of 100 kDa. Membrane material in this case was polyethersulfone. Black: Initial solution. Red: Filtrate. **A**: **Rh–SO_3**, Permeation: 55 %. **B**: **Rh–C_6SO_3**, Permeation: 1.8 %. **C**: **Rh–C_6NMe_3**, Permeation: 68 %.

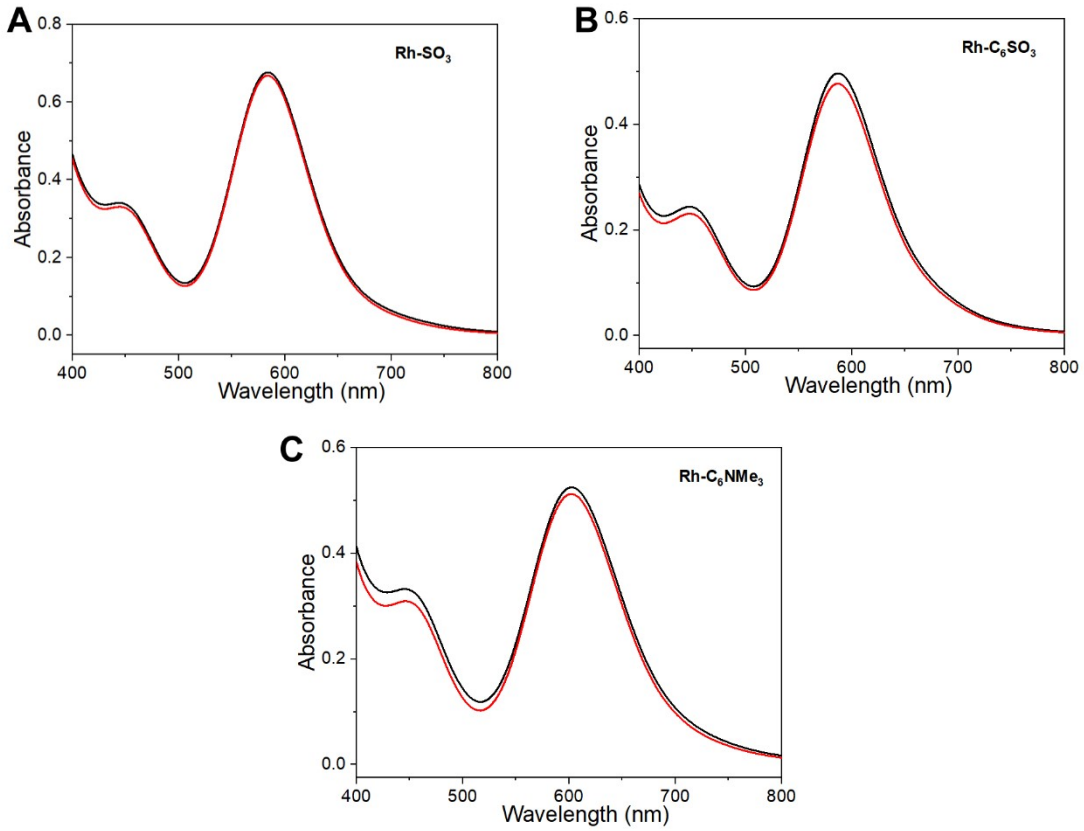

Figure S26. Determination of the permeation coefficient for ultrafiltration membranes with a molecular weight cut-off of 1 MDa. Membrane material in this case was polyethersulfone. Black: Initial solution. Red: Filtrate. **A**: **Rh–SO_3**, Permeation: 99 %. **B**: **Rh–C_6SO_3**, Permeation: 96 %. **C**: **Rh–C_6NMe_3**, Permeation: 98 %.

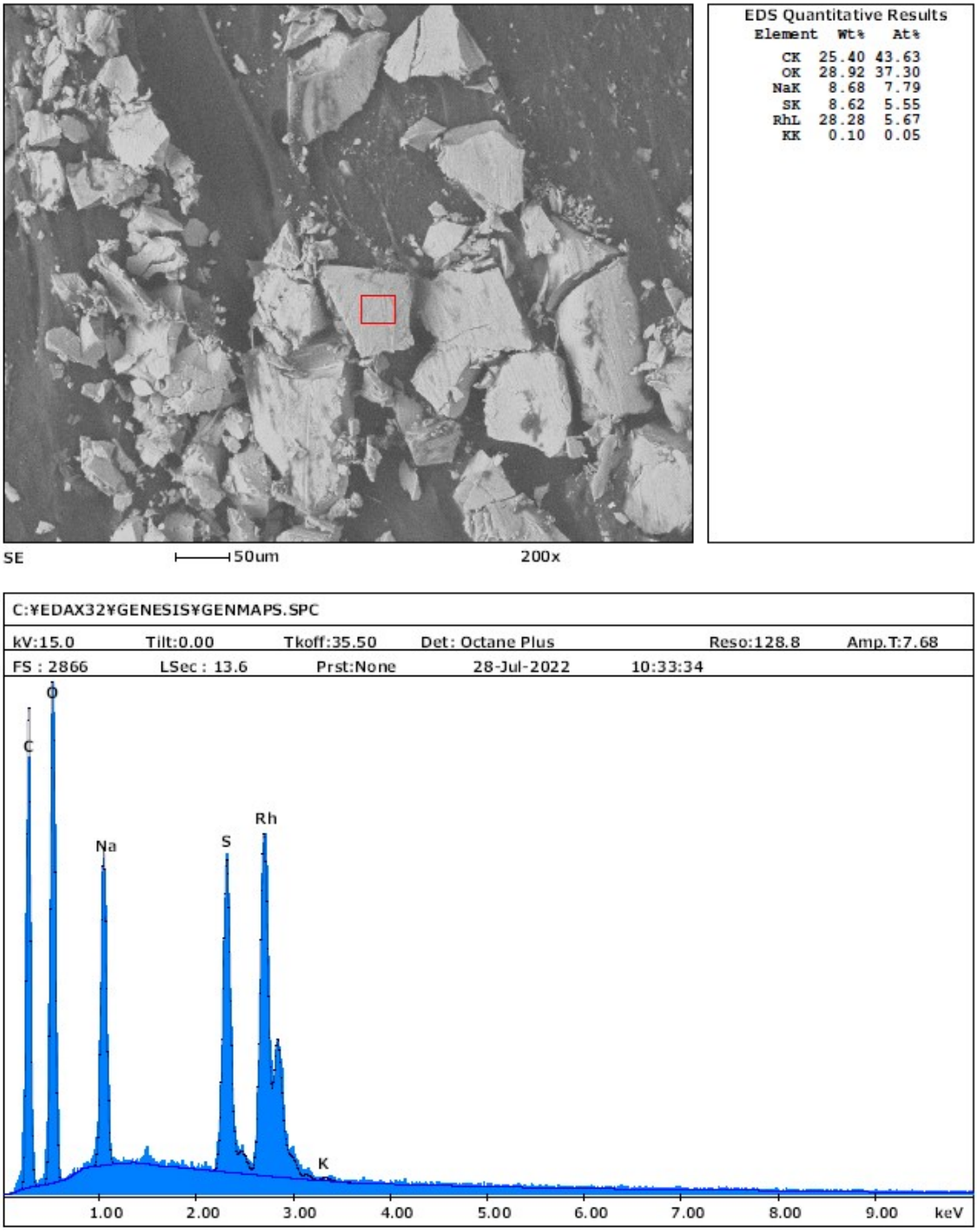

Figure S27. Representative SEM-EDX spectrum of **Rh–SO_3 (Na^+)**.

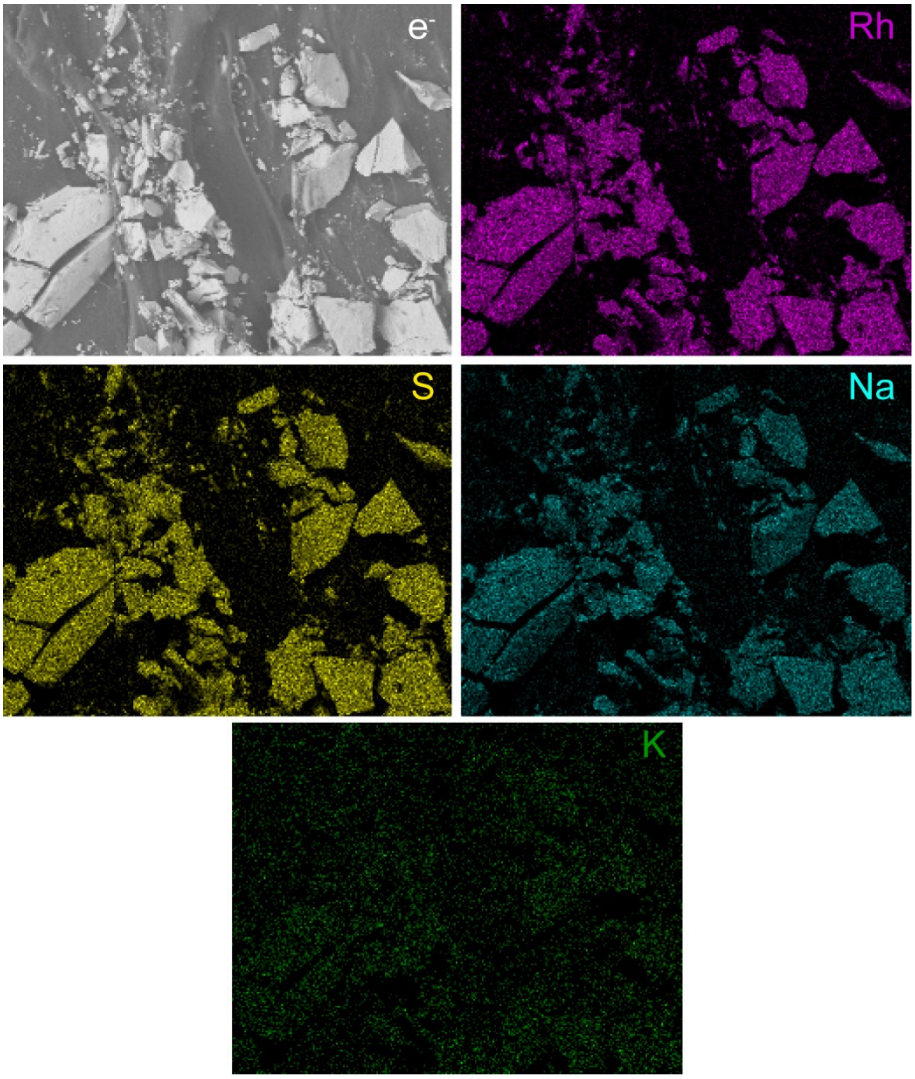

Figure S28. SEM-EDX elemental mapping of **Rh–SO_3 (Na^+)**.

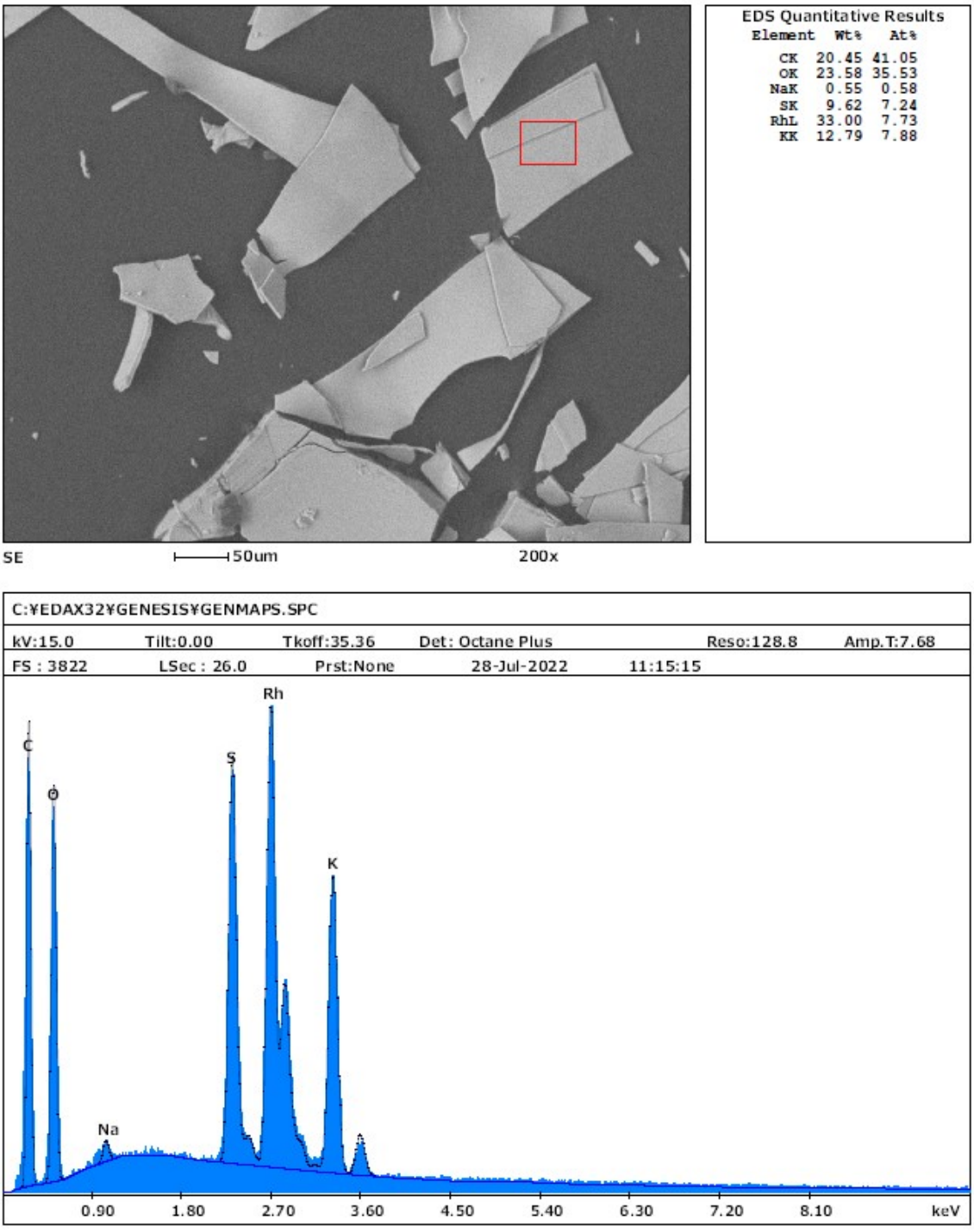

Figure S29. Representative SEM-EDX spectrum of **Rh–SO_3 (K^+)**.

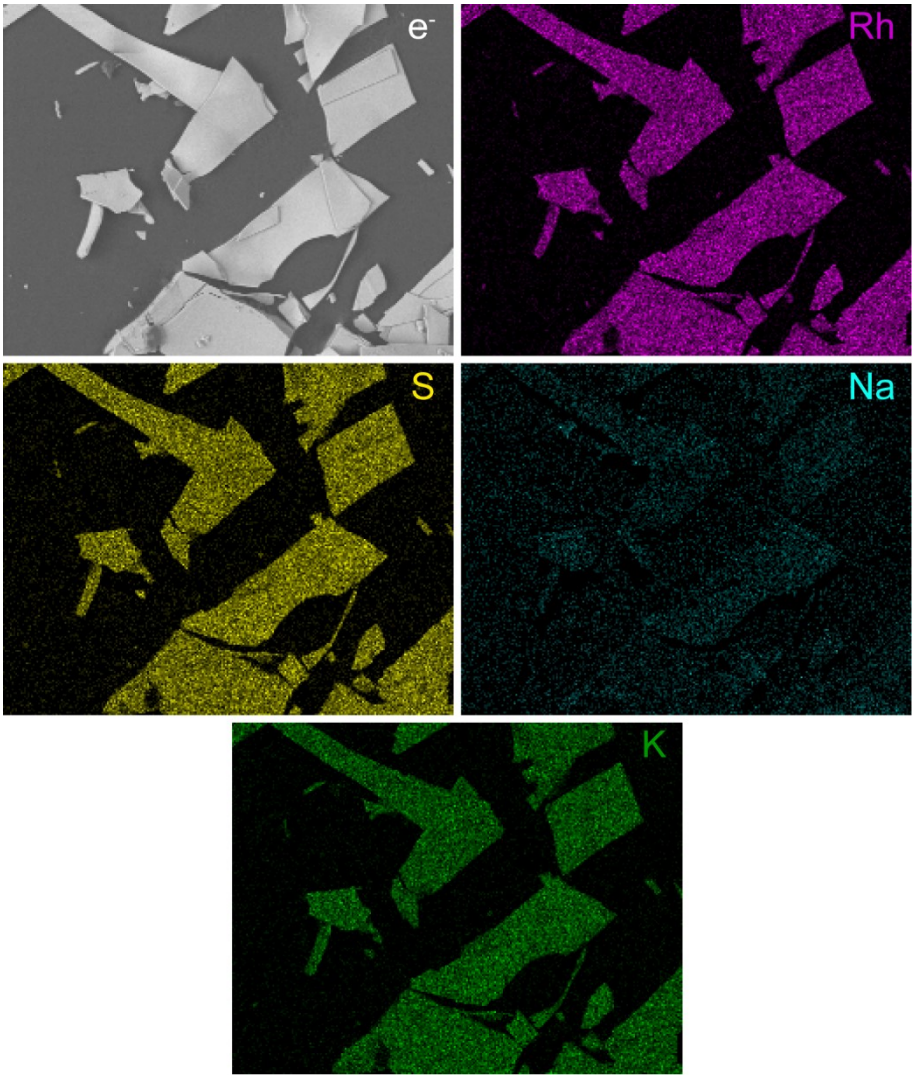

Figure S30. SEM-EDX elemental mapping of **Rh–SO_3 (K^+)**.

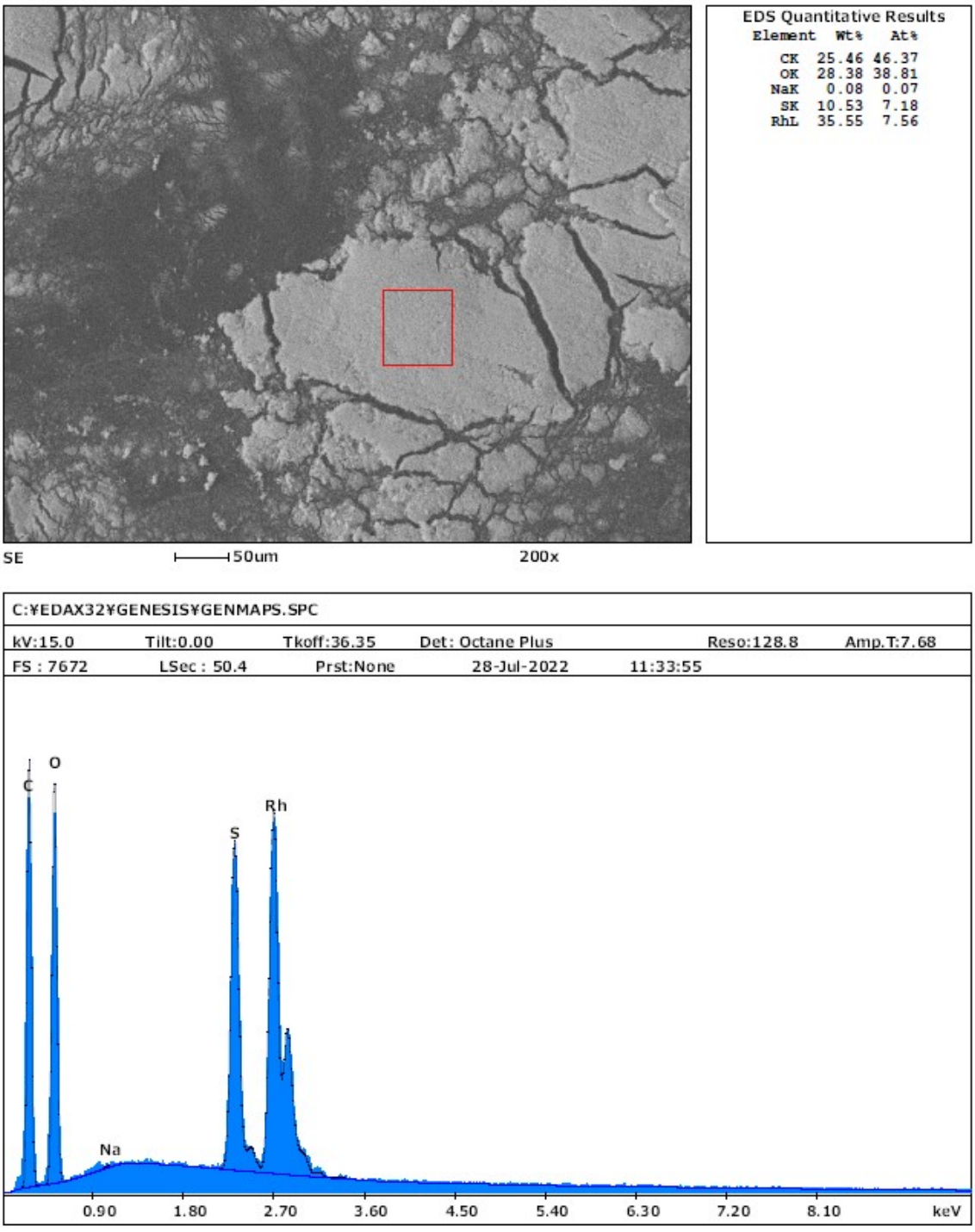

Figure S31. Representative SEM-EDX spectrum of **Rh–SO_3 (H^+)**.

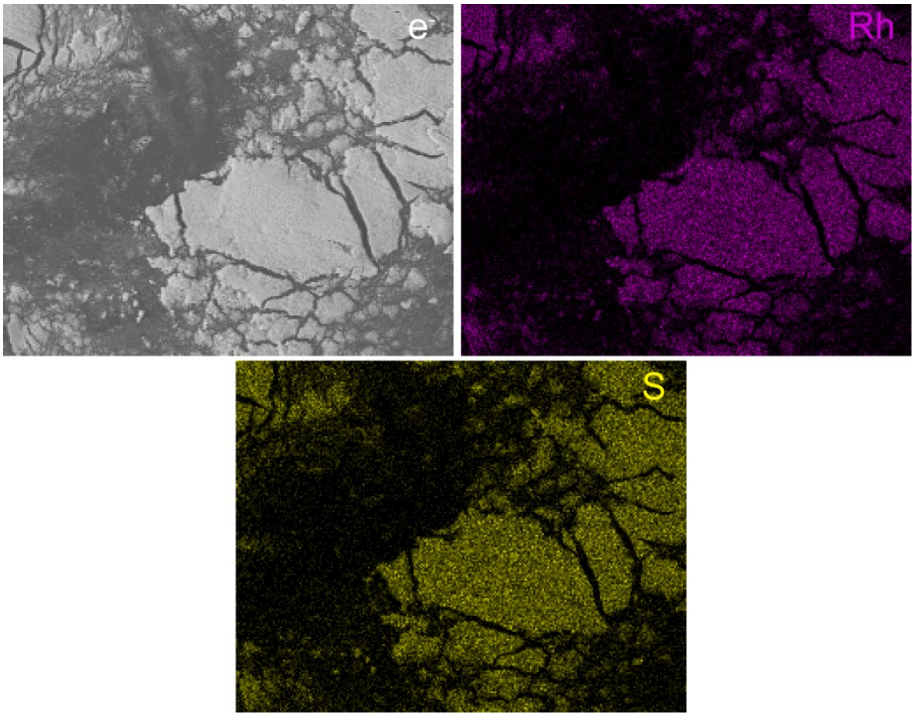

Figure S32. SEM-EDX elemental mapping of **Rh–SO_3 (H^+)**.

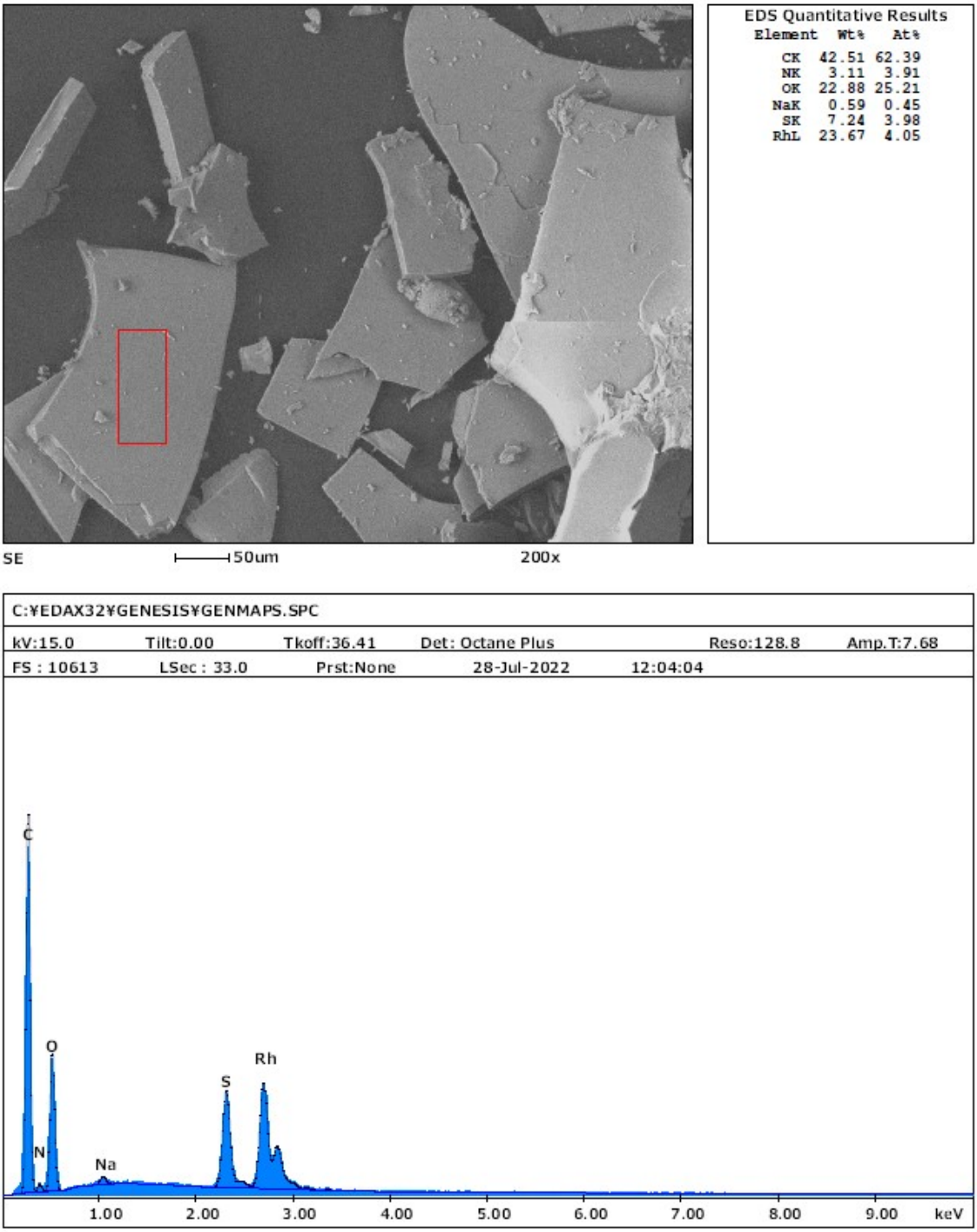

Figure S33. Representative SEM-EDX spectrum of **Rh–SO_3 (Et_4N^+)**.

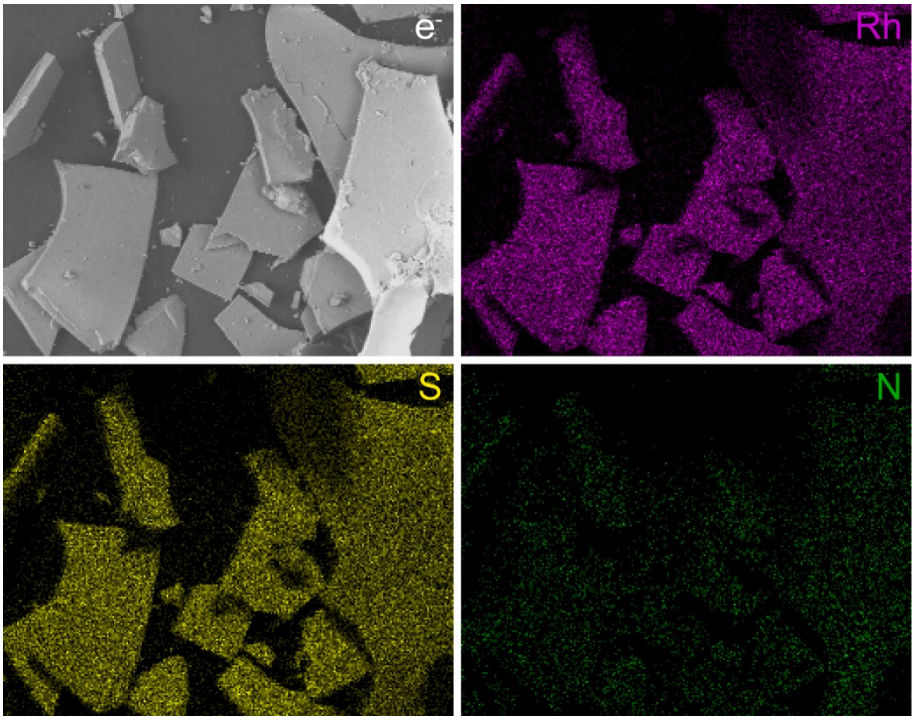

Figure S34. SEM-EDX elemental mapping of **Rh–SO_3 (Et_4N^+)**.

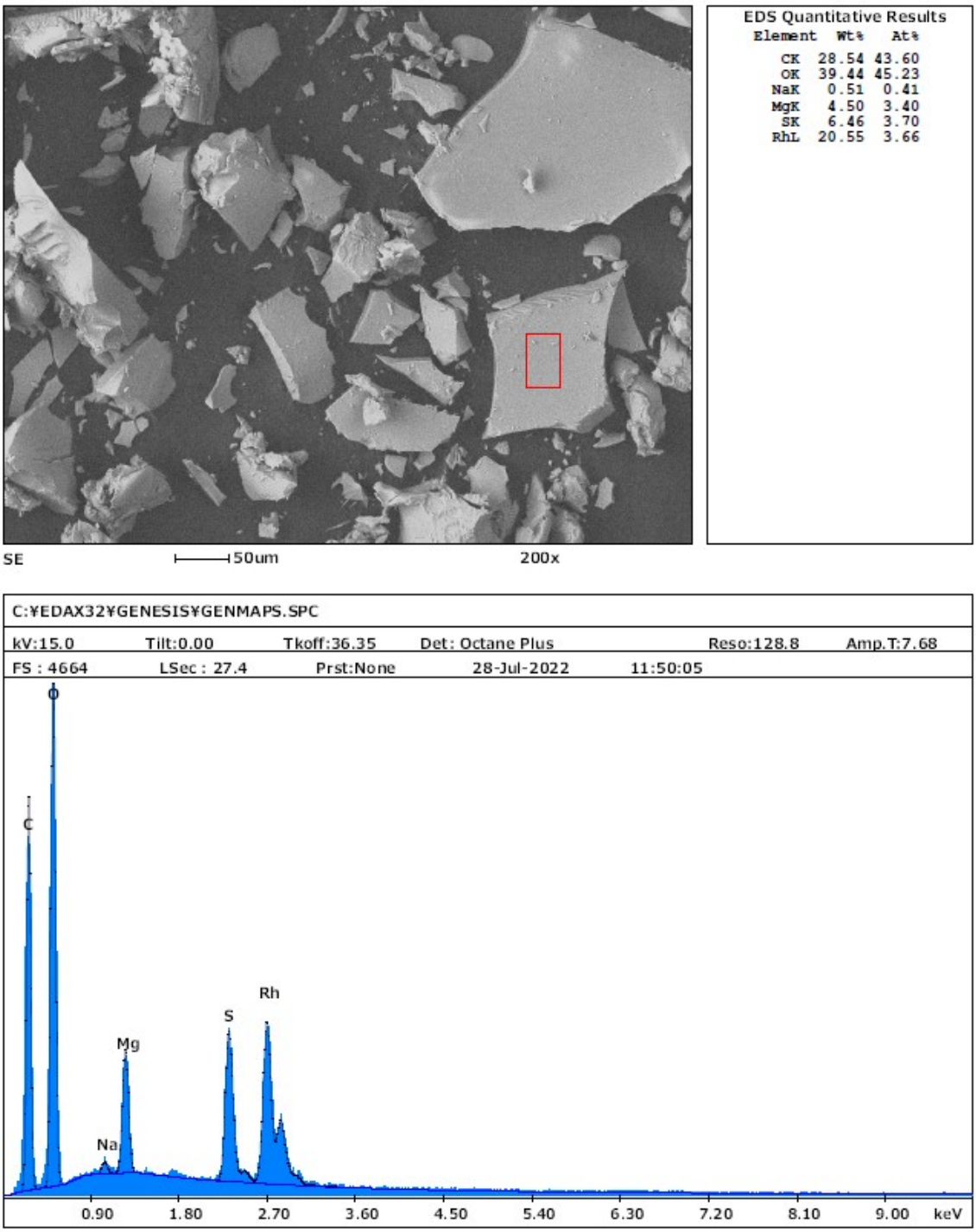

Figure S35. Representative SEM-EDX spectrum of **Rh–SO_3 (Mg^{2+})**.

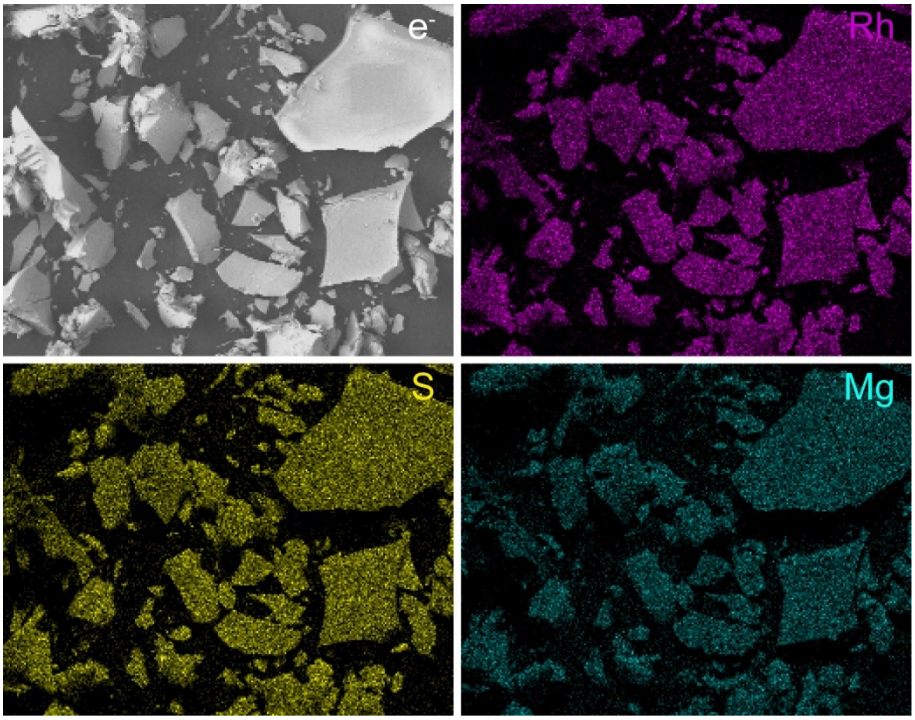

Figure S36. SEM-EDX elemental mapping of **Rh–SO_3 (Mg^{2+})**.

References

1 B. Le Ouay, R. Minami, P. K. Boruah, R. Kunitomo, Y. Ohtsubo, K. Torikai, R. Ohtani, C. Sicard and M. Ohba, *J. Am. Chem. Soc.*, 2023, **145**, 11997–12006.
2 D. Fujita, Y. Ueda, S. Sato, H. Yokoyama, N. Mizuno, T. Kumasaka and M. Fujita, *Chem*, 2016, **1**, 91–101.
3 M. Krick, J. Holstein, C. Würtele and G. H. Clever, *Chem. Commun.*, 2016, **52**, 10411–10414.